Climate and phenology drive coherent regional interannual variability of carbon dioxide flux in a heterogeneous landscape

Ankur R. Desai*

Dept of Atmospheric & Oceanic Sciences, University of Wisconsin-Madison, Madison, WI USA

*Corresponding author:

Dr. Ankur R. Desai

University of Wisconsin-Madison

Department of Atmospheric and Oceanic Sciences

AOSS 1549, 1225 W Dayton St, Madison, WI 53706 USA

Phone: +1-608-520-0305, Fax: +1-608-262-0166, Email: desai@aos.wisc.edu

Running title: Growing season timing and carbon fluxes

Submitted to *JGR-G special issue on flux upscaling*

Abstract

The climate sensitivity of plant seasonal life cycles, or phenology, may impart significant carbon cycle feedbacks on climatic change. Analysis of interannual ecosystem carbon exchange provides one way to assess this climate sensitivity. Multi-year eddy covariance carbon dioxide flux observations from five ecosystems in the Upper Great Lakes USA, located 400 km of each other and exhibiting coherent interannual variability, were used to parameterize a simple ecosystem model. The model, when properly constrained with an interannual sensitive cost function, was able to explain a significant proportion interannual variation of carbon fluxes in all ecosystems except the old-growth forest. The results reveal that spring or autumn climate thresholds impact annual carbon uptake, though the magnitude and strength varied by site. When the model was forced to maintain the same climate-phenology relationship across the five sites, most of the interannual variability could still be explained at most sites except the old-growth forest and the forest furthest in distance from the others. These results suggest that coarse spatial resolution carbon-climate models could likely specify general climate-phenological relationships at grid scales on order of 100 km without appreciably sacrificing ability to model interannual carbon cycling.

Index terms: Biogeochemical cycles, processes, and modeling (0414); Carbon cycling (0428); Biosphere/atmosphere interactions (0426)

Keywords: Phenology; eddy covariance; ChEAS

1. Introduction

One key to understanding the impacts of the terrestrial carbon cycle on future climate change is better diagnosis of climatic controls on interannual variability (IAV) of land-atmosphere carbon dioxide net ecosystem exchange (NEE). This is especially the case in temperate and boreal forests where IAV is large (Yuan *et al.*, 2009) and strongly linked to climate variability (e.g., Barr *et al.*, 2006; Chen *et al.*, 1999; Goulden *et al.*, 1996; Hollinger *et al.*, 2004; Sierra *et al.*, 2009). Large IAV could, for example, lead to reduced long-term carbon accumulation in some forests, due to the impact of disturbance-driven respiration pulses (Sierra *et al.*, 2009). Despite its importance, observed IAV of NEE in these biomes is difficult to capture in ecosystem models, which are better tuned to capture diurnal, seasonal, and successional patterns (Ricciuto *et al.*, 2008; Urbanski *et al.*, 2007; Stoy *et al.,* 2009).

Currently, we lack a strong physical basis for many of the complex interactions that exist in terrestrial systems at this timescale (Bonan, 2008; Stoy *et al.*, 2009). For example, while annual NEE typically declines with latitude in temperate regions, relative IAV increases in deciduous forests and declines in evergreen forests, a result that is difficult to explain (Yuan *et al.*, 2009). In several grasslands, it was noted that sensitivity of plant productivity to climate drivers varied year-to-year (Polley *et al.*, 2010). This result is similar to findings of Richardson *et al* (2007) who argued that biotic, not climate, variability was the primary cause of decadal flux variability in a spruce forest.

Further, we lack understanding about what scales do we expect spatial coherence in interannual variation, which may influence optimal scales of specifying climate-ecosystem relationships in land-atmosphere models. One promising avenue of research for better modeling of regional

ecosystem model IAV is improved simulation of climate sensitivity in plant phenological life cycles (Peñuelas *et al.*, 2009). Phenology links climate anomalies, especially in the shoulders of the plant growing season, to plant biogeochemistry (Morisette *et al.*, 2009; Piao *et al.*, 2008). Recent climatic warming leading to advances in spring flowering and leaf timing has been noted in many parts of the globe (Linderholm, 2006) especially in Europe (Menzel et al., 1999; Stöckli and Vidale, 2004) and North America (Myneni *et al.,* 1997; White *et al.*, 2009), across diverse ecosystems including temperate forests (e.g., Richardson *et al.*, 2006; Vitasse *et al.,* 2009) and Mediterranean shrublands (e.g., Gordo and Sanz, 2010). Climate records indicate shifts in both phase and amplitude of the annual temperature (Stine *et al.*, 2009), suggesting that links between phenology and climate will likely have significant impacts on ecosystem productivity with ensuing anthropogenic climate change. The impact of warm springs and longer growing season lengths on carbon uptake has been well-noted at several sites (Barr *et al.*, 2006; Chen *et al.*, 1999; Churkina *et al.*, 2005; Goulden *et al.*, 1996; Hollinger *et al.*, 2004), but ecosystem models that can capture this impact on IAV are elusive (Baldocchi *et al*., 2005).

One way to advance our understanding is to develop and test ecosystem models constrained by multi-year observations that connect phenology, carbon cycling, and climate at multiple sites. Long-term eddy covariance flux towers, which directly observe NEE of ecosystems over multiple years, are particularly well suited for testing how well models of phenology capture carbon cycle IAV (Richardson *et al.*, 2009), though only a few studies have used multiple flux towers (Baldocchi *et al.*, 2005; Churkina *et al.*, 2005) and none focused on multiple towers in one region. Coherent IAV has been observed across a set of flux towers in a similar climate and biome (Desai *et al.*, 2008), but there has been limited success in modeling this IAV. Here, I ask

to what extent can the observed IAV be explained by a simple climate sensitive model of plant phenology and what does it imply for improving ecosystem IAV modeling?

To investigate this question, a simple ecosystem model was developed and parameterized using Bayesian techniques against multi-year flux tower data observed in five ecosystems. Since ecosystem model interannual variability can be strongly sensitive to how parameter estimation is designed, an alternative IAV-sensitive formulation of the cost function was also investigated. Finally, to investigate controls on synchronous forcing, model parameterization was further modified to force spatial convergence on phenological parameters. Findings from these investigations are used to discuss implications for environmental controls and spatial coherence of regional IAV.

2. Data and methods

2.1 Site and data description

Eddy covariance flux towers in the temperate-boreal transition region of the Upper Great Lakes were analyzed in this study (Table 1). The sites, which included three forests, one shrub wetland, and one tall tower regional mixed forest-wetland footprint, were located within 400 km of each other (Fig. 1), each have at least five years of flux and meteorological data, and have been previously analyzed and described in an upscaling study (Desai *et al.*, 2008). Four of the sites (US-WCr, US-Syv, US-Los, and US-PFa) are within 150 km of each other in north central Wisconsin/upper Michigan, while the fifth site, US-UMB, is in northern Lower Michigan. Of the forest sites, two are mature age class (US-WCr and US-UMB), and one is old-growth (US-Syv). The wetland site is a short-stature shrub alder-willow fen. The tall tower is a 447-m radio tower

with flux measurements at three heights. For the purposes of this comparison, the fluxes from the three levels of the tall tower are combined in an optimal selection strategy, as described by Davis *et al.* (2003), to produce a single "regional" NEE.

Meteorological data are each site were acquired and gap-filled using a combination of nearest neighbor and moving-window ensemble diurnal average techniques (Desai *et al.*, 2008). Eddy covariance and storage fluxes of CO_2 were used to compute NEE at each site. Standard flux computation methods at each site were relatively similar (Desai *et al.,* 2008) and fluxes computed by these codes have compared favorably to the Ameriflux "gold" standard, a network-wide blind data processing protocol. Common techniques were used in screening for low turbulence conditions and gap filling of data gaps that occur due to low turbulence or instrument failure (Desai *et al.*, 2005). The gap-filling technique compared well with other standard techniques used by the flux tower community (Moffat *et al.*, 2007). All fluxes were computed at the half-hourly scale, except for US-PFa, which used an hourly scale due to the taller height. For assimilation into the model, all flux and meteorological data were averaged across day and night periods, similar to the method of Sacks *et al.* (2006). Using half-daily summed fluxes reduces impact of random turbulent flux error on data assimilation, but retains the nocturnal respiration signal. Summed half-daily flux integrals whose hours were more than 25% gap-filled were discarded for data assimilation to minimize artifacts arising from model-model comparison.

2.2 Model description

A simple ecosystem model, the Interannual Flux Tower Upscaling Experiment (IFUSE), was parameterized against all site data. The model consisted of 17 total parameters (Table 2), of which 3 were fixed for each site, 10 were optimized at each site, and four phenology parameters

124 were either optimized at each site separately (asynchronous mode) or jointly for all sites
125 (synchronous mode). The model was run at a half daily (day/night) adaptive length time step,
126 which has been shown to be well suited for parameter optimization against flux tower NEE
127 (Sacks *et al.*, 2006).

128 At each time step, the model applied environmental forcing of canopy air temperature (T_a), 5 cm
129 soil temperature (T_s), photosynthetic active radiation (PAR), and vapor pressure deficit (VPD) to
130 estimate gross primary production (GPP), ecosystem respiration (ER), and NEE in gC m^{-2}
131 $timestep^{-1}$ and leaf area index (LAI) in m^2 m^{-2}. GPP was estimated using a five-parameter light,
132 temperature, and VPD limited modified light use efficiency equation:

133 $$GPP = LUE \cdot \left(1 - e^{-k \cdot LAI}\right) PAR \left(\frac{T_a - T_{\min}}{T_{opt} - T_{\min}} \right) \left(\frac{VPD_{\max} - VPD}{VPD_{\max} - VPD_{\min}} \right) \quad (1)$$

134 where LUE, k, T_{min}, T_{opt}, VPD_{max}, and VPD_{min} are model parameters as described in Table 2.

135 To calculate LAI, leaf phenology of emergence and senescence was modeled with a two-
136 parameter sigmoidal relationship. The phenology model used here consisted of the well-
137 established accumulated growing degree days base 10 C (GDD) approach for mid-point of leaf
138 emergence and a 5 cm soil temperature threshold for mid-point of leaf senescence, models which
139 have been shown to explain much of the variation in canopy development for northern forests
140 (Baldocchi *et al.*, 2005; Richardson *et al.*, 2006). Canopy fraction with evergreen vegetation was
141 simulated by preventing LAI to decline beyond a minimum threshold (LAI_{min}), leading to:

142
$$\begin{cases} LAI = LAI_{\min} + \left[\left(LAI_{\max} - LAI_{\min} \right) L_{spring} L_{fall} \right] \\ L_{spring} = \dfrac{1}{e^{-\alpha\left(DOY - \frac{L_{on}}{2} \right)}}; L_{fall} = 1 - \dfrac{1}{e^{-\beta\left(DOY - \frac{L_{off}}{2} \right)}} \\ L_x = \dfrac{L_x - \min(L_x)}{\max(L_x) - \min(L_x)}; x = spring \,/\, fall \\ L_{on} = DOY\big|_{GDD > GDD_{Thresh}}; L_{off} = DOY\big|_{T_s < T_{Thresh}} \cup L_{spring} > 0.99 \end{cases} \quad (2)$$

143 where LAI_{min}, LAI_{max}, α, β, GDD_{thresh}, and T_{thresh} are model parameters (Table 2). L_{spring} and L_{fall}
144 describe the variation of LAI around the leaf on (L_{on}) or leaf off (L_{off}) day of year (DOY). Both
145 of these functions were further normalized to vary between 0 and 1 and then multiplied together,
146 thus allowing LAI to vary between LAI_{min} and LAI_{max}. Consequently, interannual variability in
147 LAI is quite muted in this model, which allowed this model to focus on the role of growing
148 season length (G_{SL}) on IAV of NEE.

149 ER was estimated with five parameters that control respiration rates in three soil pools sensitive
150 to T_s, T_a, and GPP:

151
$$ER = \left[r_s \cdot e^{b_1 (T_s - 15)} \right] + \left[r_v \cdot e^{b_2 (T_a - 15)} \Big|_{GPP > 0} \right] + \left[b_3 \cdot GPP_{DOY-1} \right] \quad (3)$$

152 where r_s, r_v, b_1, b_2, and b_3 are model parameters (Table 2). The first term represents the combined
153 effects soil heterotrophic and plant maintenance respiration. The second term, which is only
154 present when GPP is positive, represents plant growth respiration (or alternatively, the change in
155 respiration sensitivity in growing vs. dormant seasons), while the final term, is a fraction of the
156 previous day GPP, representing autotrophic respiration of newly assimilated carbohydrate and
157 allows for GPP lag effects. These formulations were chosen to represent the dynamics that could

158 likely be resolved from NEE measurements, as opposed to a more mechanistic, but also more
159 parameter intensive and pool sensitive model of respiration.

160 NEE was computed as the residual between ER and GPP. The model was designed to be
161 purposefully simple so as to capture the key diurnal and season dynamics typically seen in NEE
162 observations while limiting the number of parameters. By avoiding specification of soil and
163 biomass pools outside of leaves, the model removed one of the largest sources of uncertainty and
164 equifinality in estimating model parameters from flux data (Luo *et al.*, 2009). This structure
165 implied that soil pools were assumed to be steady state relative to the fluxes, which is likely a
166 reasonable assumption for mature, established secondary succession ecosystems. Since the goal
167 was simulation of daily to interannual NEE at timescales less than a decade (i.e., <10% of a
168 temperate hardwood forest successional cycle), this assumption implied that short-term
169 variations in NEE were driven entirely by the response of ER and GPP to climate. Given the
170 mesic climate of the region, influences of precipitation and moisture variability were assumed to
171 be minimal. The impact of these assumptions on interpretation of results is provided in the
172 discussion.

173 ### *2.3 Model parameterization*

174 Free parameters of the model (phenology, photosynthesis and respiration parameters in Table 2)
175 were estimated using a Markov Chain Monte Carlo (MCMC) estimator (Braswell *et al.*, 2005)
176 with the Metropolis-Hasting algorithm (Metropolis and Ulam, 1949). In this approach, free
177 parameters were randomly perturbed across a range of reasonable prior values, assuming a
178 uniform distribution (Table 2). New parameter sets were "accepted" when a cost function
179 indicated better fit of model to data, and occasionally when not, so as to avoid local minima.

Multiple chains (six, in this study) were built from random locations in parameter space and iterated until a convergence criterion is reached, usually within 50,000 iterations. Iteration sizes were chosen to be arbitrarily large, likely oversampling the parameter space. The best chain was then propagated forward another 70,000 iterations, and a subset of the final 80,000 iterations were saved as "accepted" parameter sets based on the acceptance criterion. Best model output and variance were computed from the model output of these accepted parameter sets. More details of the general approach are provided in Braswell *et al.* (2005).

The first five years of half-daily NEE observations for each site were used in the MCMC cost function to minimize model-data mismatch. The cost function can be written as:

$$L_D = \prod_{i=1}^{n} \frac{1}{\sqrt{2\pi}\sigma} e^{\frac{-(x_i-\mu_i)^2}{2\sigma^2}} \quad (4)$$

where L_D is the likelihood to be minimized, x_i is observed half-daily NEE, u_i is model NEE, and σ^2 is data error with respect to model structure, which was computed as the mean sum of square deviations between x_i and u_i (Sacks *et al.*, 2006). To improve numerical stability, this equation was computed as the log likelihood, allowing the product function to be written as a sum. Additionally, to test whether the cost function biases how well the model identifies parameters responsible for determining carbon flux IAV, Eq. (4) was further modified to account for both fast (half-daily) and slow (annual) variations in NEE:

197
$$\begin{cases} L_y = \prod_{i=1}^{n} \frac{1}{\sqrt{2\pi}\sigma} e^{\frac{-\left(x_i^m - \mu_i^m\right)^2}{2\sigma^2}} \\ x_i^m = \sum_{j=i-DOY}^{i} x_i ; \mu_i^m = \sum_{j=i-DOY}^{i} \mu_i \\ L = L_D L_y \end{cases} \quad (5)$$

198 where L_y is a likehood for annual NEE, and x_i^m is observed cumulative NEE from the start of the
199 year to point i, and u_i^m is the equivalent for the model. The new cost function is then product of
200 the two likelihoods. Thus the model trades fit at the daily scale for fits at the annual scale, with
201 the assumption that accepted parameters sets would be Pareto optimal for both. Cumulative NEE
202 was used instead of annual NEE to allow for both the daily and annual to have roughly the same
203 weight and also to prevent the model from fitting annual NEE with a poor seasonal pattern. The
204 expectation is that this cost function may improve model reproduction of seasonal NEE and IAV
205 without significant loss in explaining short-term variation. While L_d was weighted to account for
206 the influence of gap-filled data by removing half-daily NEE sums with more than 25% gap-
207 filled, L_y included all NEE to create well-formed NEE integrals. In most cases, this did not add
208 significantly more points or appear to bias results.

209 In addition to the two cost functions above, an alternate optimization was performed where
210 phenology parameters (Table 2) were forced to be the same for all five sites. In this "synchrony"
211 setup, the parameter optimization was run in tandem at all five sites, such that the four phenology
212 parameters were optimized to be the same at all five sites, while the other ten parameters were
213 allowed to vary by site. Computationally, this was simply performed by concatenating arrays of

flux and forcing data for all sites, with 5 sets of 10 independent parameters (50), and 4 co-dependent parameters. Thus a single MCMC run estimated 54 parameters, instead of 14 at a time for each site. To compensate for the larger number of parameters, the number of chains was increased to 20 and total iterations to 432,000 (with 144,000 spin-up iterations). Since phenology parameters were jointly modified at all five sites, the optimized phenology parameters were the same at all sites in the synchrony optimization.

2.4 Experimental design

Given the two cost functions, and two forms of parameter optimization (asynchronous and synchronous), a total of three out of four experiments or model modes were analyzed here. These include asynchronous optimization with the Eq. (4) half-daily cost function ("A_H"), the asynchronous optimization with the Eq. (5) interannual cost function ("A_I"), and finally a synchronous optimization with the Eq. (5) cost function ("S"). Results from the fourth, synchronous optimization with the daily cost function, were performed but not discussed here since the results are nearly identical to the A_H experiment. The three experiments provide information about how well IAV can be parameterized and simulated at five sites by a simple ecosystem model (experiments A_H and A_I) as well as test how important synchronous phenological forcing drives coherent IAV (experiment S).

3. Results

3.1 Seasonal patterns

Mean annual NEE at the five sites ranged from a large carbon sink (negative) to a moderate source (positive) of CO_2 to the atmosphere (Table 1). Mature forests such as US-WCr and US-

UMB were the largest sinks followed by the shrub wetland (US-Los). In contrast, the old-growth forest (US-Syv) was near neutral (with large fluctuations between source and sink in any one year), and the mixed regional very tall tower (US-PFa) was the largest source. While the regional CO_2 source observed by the tower has been a continuing puzzle (see Davis *et al.*, 2003 and Ricciuto *et al.*, 2008 for further discussion and Desai *et al.*, 2010 for a regional perspective), the other towers have NEE in line with expectations for vegetation type and latitude (Yuan *et al.*, 2009). Uncertainty arising from random error, gap-filling and low-turbulence filtering was generally small and similar at all sites.

Despite large variations in annual NEE, mean seasonal patterns at all five sites were quite similar (Fig. 2, black line). Generally, sites started absorbing carbon in late May/early June, and crossed zero in cumulative NEE by mid-June, and turned back into carbon sources by late August or early September, except for US-PFa which turned into a carbon source much earlier in August. While the dates were similar for each site, small variations in those dates led to large differences in the length of carbon uptake period, with the largest at the mature forests and wetlands, and shortest in the old-growth forest and regional site. This finding provides one basis that growing season timing and length were a strong controlling factor of annual carbon flux, and hence IAV.

When compared to seasonal flux tower NEE, the IFUSE model (averaged across the same years as observations) generally replicated this pattern regardless of optimization mode (Fig. 2, dotted and gray lines). In all cases, the A_H experiment best replicated half-daily variations in NEE, explaining 83%-93% of variability (Table 3), followed in most cases by A_I, except at US-UMB, where the S model outperformed A_I. Both A_H and A_I performed worst at US-PFa, perhaps because of the mixed footprint, while the S model performed worst at US-Syv. All modes underestimated the strength of growing season uptake at US-PFa. Differences of model

258 performance due to change in cost function are discussed in the next section. Visually (Fig. 2), it
259 is apparent that the A_I model better captured seasonal variation than A_H at most sites, especially
260 at US-Syv, but for magnitude of annual NEE, all modes did well with respect to uncertainty in
261 observations, except for A_H at US-Syv.

262 ### *3.2. Interannual variability*

263 IAV at all sites was present and ranged from modest in the case of the wetland, to large in the
264 case of the mature and old-growth forests (Table 1). When mean annual NEE is subtracted from
265 observations and the anomalies are then normalized by standard deviation, consistent patterns
266 emerge among the sites (Fig. 3). At most sites, IAV rarely exceeded 1-σ, with the exception of
267 2001, coincident with a large regional forest tent caterpillar outbreak (Cook *et al.*, 2008). Year-
268 to-year fluctuations were quite common, and hints of a longer decadal scale variability were
269 evident. The spatial coherence of these anomalies are discussed in the next section.

270 No relationship existed between NEE magnitude and 1-σ IAV (Table 3). In absolute terms, IAV
271 was smallest in the wetland, barely detectable within the uncertainty in mean NEE, and largest at
272 US-WCr, the site most impacted by the 2001 insect outbreak. However, in relative terms (ratio of
273 1-σ IAV to NEE), the largest IAV was at US-Syv, where NEE was near neutral. In all cases,
274 IAV was a major fraction of NEE.

275 Despite all modes being able to capture most of the seasonal pattern of cumulative NEE at all
276 sites, simulation of IAV anomalies was poorly modeled at all sites by A_H (Fig. 4a), but
277 significantly improved in A_I (Fig. 4b). This result highlights the importance of the dual-
278 likelihood cost function used by A_I. A_I IAV anomalies were significantly correlated ($p<0.05$) to

observed IAV anomalies at US-WCr, US-UMB, and US-PFa, strongly correlated ($p<0.1$) to US-Los, and weakly correlated to US-Syv (Table 3). The tradeoff, of course, was loss of explanation of variance at the half-daily scale ranging from 3-11% and an increase in mean absolute error of half-daily NEE by 0.03 to 0.3 gC m^{-2} day^{-1}.

Further evidence that the fit of A_I to observations is not just an artifact of modeling comes when A_I L_{on} and L_{off} dates were compared to similar data observed at US-WCr. The observed dates were derived from calibrating a simple LAI model to the ratio of above and below canopy downwelling PAR and observed LAI (Cook *et al.*, 2008). While correlations are modest, the model generally captured the pattern of anomalies in L_{ON} and L_{OFF}, though it did appear to underestimate the variability in L_{on} and overestimate the variability in L_{off}. The net effect, however, was good performance at simulating variations in growing season length.

In parameter space, there are a number of differences between A_H (Table 4) and A_I (Table 5). Among phenology parameters, the net effect was in most but not all cases to increase the values of phenology slope parameters, α and β, to higher values (steeply curved), consequently modifying the phenology climate thresholds. Covariances between these parameters and photosynthesis parameters then led to changes in LUE and temperature regulation of photosynthesis, since these parameters can also act like phenology parameters. Less clear were the reasons behind large changes in respiration parameters. While both A_H and A_I essentially optimized to a value of zero for b_3 (fraction of GPP respired), A_I has significantly smaller b_2 (less temperature sensitivity for plant growth respiration), and some large differences for b_1 for the mature forest sites, suggesting equifinality in model solutions for respiration and highlighting the difficulty of estimating optimal respiration parameters from eddy covariance data.

3.3 Synchronous forcing

While the magnitude of NEE and IAV varied across sites and with time, coherent anomalies in IAV were readily observed when anomalies were statistically standardized (Fig. 3). These results indicate the strong role that regional climate variability had on IAV. Even after taking NEE uncertainty into account, coherence was strong, with most sites showing positive anomalies in 2001 and 2004, and negative anomalies in 1999-2000, and 2002-2003. A bifurcation of trends across sites occurred in 2005 and 2006. While the tent caterpillar outbreak was one source of the anomaly in 2001, the outbreak was mostly felt at US-WCr in late spring, to a small extent in the US-PFa footprint, and barely at the other two sites, suggesting that climate anomalies still explained most of the 2001 anomaly.

The S model tested whether synchronous IAV can be explained by coupling of phenological parameters across sites. In this synchronous mode, the model still captured much of the IAV at US-WCr, US-Los, and US-PFa ($p<0.05$), but lost ability to simulate IAV at US-UMB, and like all modes, could not capture IAV at US-Syv (Table 3). Correlation coefficients for the significant correlations were essentially unchanged compared to A_I. It is interesting to note that US-UMB is the further site from the rest (Fig. 1).

The trade-off in half-daily NEE simulation compared to A_H was quite similar to the trade-off found for A_I, though with a larger drop in correlation at US-Syv. Across all sites, A_I has a strong correlation with observed IAV ($r^2=0.81$) (Fig. 4b), but the S mode is still strongly correlated ($r^2=0.68$), and with 16 fewer parameters in aggregate compared to A_I. Photosynthesis and respiration parameters in A_I (Table 5) and S (Table 6) were more similar than between those and A_H (Table 4). Remarkably, the parameters in S appeared more in line with literature estimates

than those for A_I, especially T_{opt}. Phenology parameters in S are fixed for all five sites, and appeared to fall roughly near the average of those parameters for each site in A_I.

4. Discussion

4.1 Modeling of IAV

The observed IAV is within the range (~50-100 gC m^{-2} yr^{-1}) observed for deciduous broadleaf forests in mid-latitudes (Yuan *et al.*, 2009), with mature northern hardwood forests exhibiting the largest. The results here contribute to findings of interannual variations in seasonal temperature as a dominant driving force of interannual variation in carbon flux at mid-latitudes (Sierra *et al.*, 2009; Yuan *et al.*, 2009). Given the observed coherent IAV across space and likelihood that seasonal temperature fluctuations were important in the study region, then, it is not entirely surprising that a model tuned to capture daily to seasonal climate sensitivity of carbon cycling can adequately capture the observed IAV, especially given that seasonal climate forcing strongly influenced modeled ecosystem growing season length and timing. Rather, what is surprising is the level of care needed for proper parameterization and the importance of not just identifying optimal model structure and parameters, but also optimal model cost functions. In this case, as in many ecosystem models, the failure of a simple MCMC approach in tuning parameters for simulating IAV relies partly on the large signal imparted by CO_2 flux diurnal variability (large and negative in day, large and positive at night), which tends to mask the more subtle, but perhaps more climatically relevant, interannual signal (Stoy *et al.*, 2009).

The simulation presented here, consequently, is one of few models that have been able to successfully diagnose interannual variability of NEE within a relatively simple ecosystem model.

Other well-known, and arguably more sophisticated models have shown less ability to model IAV in north temperate forested regions (Ricciuto *et al.*, 2008; Urbanski *et al.*, 2007). It is likely, at least in the case of the northeastern forest studied by Urbanski *et al.* (2007), that successional trajectory was an important factor in long-term variability at the site, possibly overwhelming a climate variability signal. A major shortcoming of the approach used here is the inability to estimate how important succession and disturbance is part of sub-decadal IAV. Investigations at decadal or longer timescales would certainly need to incorporate these process. Further, the steady-state spin-up assumption made by developing a model with no carbon pools would not be valid, and other techniques should be implemented with a pool based model (e.g., Carvalhais *et al.*, 2008).

Analysis also revealed large variation in IAV variance explained by this model within a small region that appeared to vary as a function of vegetation type, highlighting the importance of individual site characteristics in determining the extent to which interannual carbon cycling may be more controlled by climate or internal biotic dynamics (Polley *et al.*, 2010). Strong internal control of NEE variability appears to have played a part in the lack of model predictive ability at the old-growth forest. Desai *et al.* (2005) also highlighted the greater sensitivity to moisture stress that has been found at this forest compared to nearby mature forests.

One way to assess biotic control that has been demonstrated both by Polley *et al.* (2010) and Richardson *et al.* (2007), is to compare model parameterization with fixed parameters over multiple years against interannually varying parameters, the latter reflecting variability in biotic controls on NEE. Polley *et al.* (2010) argued that biotic control of interannual variability was significant in grasslands, and Richardson *et al.* (2007a) similarly argued that the majority (55%) of interannual variations in a spruce forest in the northeast US was driven by biotic variation.

Though this study did not test a model with variable parameters, the findings here of strong explanation by a simple model with fixed-in-time parameters suggests that, at least for mature hardwood forests of boreal-temperate transition reasons, climate sensitivity, especially of spring and fall, drove interannual variation of NEE.

While model was able to simulate IAV at the wetland, it was more designed with forest productivity and aerobic decomposition in mind, suggesting non-shrub or precipitation-fed wetlands would not fare as well as the shrub fen studied here. Still, this particular wetland site was not in steady state over the time period due to a significant ongoing decline in water table (Sulman *et al.*, 2009). Sulman *et al.* (2009) showed that water table influences both respiration and productivity this wetland, generally leading to little change in NEE over the time period studied. Consequently, one could argue that this model may be getting the right answer for the wrong reasons, given the relatively small interannual variability of NEE.

Differing model structures led the MCMC algorithm to select different optimal values for many number of parameters. When the models were compared in parameter space, it was not always immediately obvious how other parameter differences between the models improved the fit to IAV. These parameter correlations require further examination and suggest that caution is required when drawing inferences from model parameter optimization techniques without first testing for optimal model structure. Additionally, a question of overfitting to IAV arises when relying on datasets with only a few years of data and the modified cost function, which also requires further examination.

4.2 Synchronous phenological forcing

Another major finding of the work here is the how well a synchronously forced phenology explained much of the IAV in the region for forests. Though the details of plant phenology vary strongly by species and microclimate experienced by individual plants, at the scale of stand-level carbon cycling, results here suggest that carbon cycle responses can generally be estimated by relatively simple accumulated climatic heating indices and regional soil temperature thresholds. Within this framework, it is not surprising that the US-UMB site fared poorest under synchronous forcing, as it is the farthest site both climatically and geographically from the other sites. These results also hint at a possible way to better estimate the spatial coherence of phenological forcing by utilizing sets of flux towers to geostatistically test the ability of models to jointly simulate flux variability. Here, the findings suggest synchronous scales of at least 100 km, reflecting the distance among the tower sites outside of US-UMB. Also, the decline in explanation of variance at the old growth forest further develops the case that this site has strong internal control on interannual carbon cycling.

4.3 Carbon cycling and growing season length

The parameterized A_I model can be further examined to suggest mechanisms that connect climate variability to flux variability, via the interaction of model parameters that impact growing season length (Fig. 7). For sites where the A_I model successfully simulated IAV, the mechanism of by which phenology impacted IAV was not consistent across all sites. Hardwood forest sites (US-WCr and US-UMB) showed less carbon uptake (more positive NEE) with later L_{ON}, while other sites had no significant relationship (Fig. 7a). For these two sites, the strength of this L_{ON} relationship drove a negative relationship between growing season length (G_{SL}) and

409 NEE (longer G_{SL} = more uptake). This finding is consistent with previous single site studies that
410 have noted relationships between warmer springs and enhanced annual carbon uptake in a boreal
411 aspen forest (Barr *et al.*, 2006; Chen *et al.*, 1999), eastern deciduous forest (Goulden *et al.*,
412 1996), and a spruce-dominated eastern forest (Hollinger *et al.*, 2004; Richardson *et al.*, 2009).

413 The effect of autumn (L_{OFF}) is less clear, with one only forest (US-Syv) showing a significant
414 positive relationship (later L_{OFF} = less uptake) (Fig. 7b). The wetland site (US-Los) also had a
415 significant relationship, but the magnitude was very small. A recent paper noted that warmer
416 autumns led to less carbon uptake in boreal ecosystems, by increasing ER more than GPP (Piao
417 *et al.*, 2008). This effect is not strongly evident here in the temperate-boreal transition zone.
418 While strong consistent spring and autumn climate impacts on NEE were not apparent, the effect
419 of both of these effects on G_{SL} is significant and negative (longer growing season = more carbon
420 uptake) at all sites except the mixed regional site (US-PFa), consistent with earlier findings
421 across the flux tower network showing growing season length as a strong determinant of net
422 carbon uptake (Baldocchi *et al.,* 2001; Churkina *et al*., 2005). The lack of strong correlation at
423 the US-PFa site may be related to complementary responses occurring across the mix of stand
424 types sampled by the tall tower and perhaps the influence of moisture on regional fluxes that is
425 not apparent at the stand-scale towers (Desai *et al.*, 2010).

426 With respect to moisture, there is some evidence to suggest that relationships between water and
427 carbon cycle are an important factor on IAV to consider. Hu *et al.* (2010) found that evergreen
428 montaine forest carbon uptake had an inverse relationship with growing season length, due to the
429 importance of snowmelt as a source of growing season plant available water. The findings here,
430 showing mostly the opposite case, do not suggest a strong control of snow water on IAV in the
431 study region. However, other studies in the region have shown that water table depth (Desai *et*

al., 2010; Sulman *et al.*, 2009) and summer soil moisture (Ricciuto *et al.*, 2008) may also be important factors in explaining IAV in the patchy forest-wetland landscape that characterizes the region, and in similar forests of other regions (Hollinger *et al.*, 2004). Ricciuto *et al.* (2008) noted that daytime and seasonal NEE at the regional tall tower (US-PFa) were correlated to soil moisture, but correlations were weak at the annual scale. The models used here did not consider these effects, which may explain some of the unexplained variability of IAV, especially at the wetland and old-growth forest. Time lags are likely in relationships between moisture and carbon (e.g., Desai *et al.*, 2010; Dunn *et al.*, 2007; Hu *et al.*, 2010), and model mechanisms to couple these processes require further assessment.

5. Conclusion

Thirty-one site years of near continuous flux tower carbon exchange observations across a meso-network of five established Ameriflux sites were used to identify a coherent signal of interannual variability in net ecosystem exchange, a likely indicator of the role of regional climate variability on ecoystem carbon cycling. A model parameterized with climate-sensitive phenology and a minimal set of carbon cycle functions and parameters to explain daily variations in NEE could successfully simulate much of this IAV, especially at the mature forest sites, but only when the model cost function was correctly identified and applied.

Climate variability in this boreal-temperate transition region drove NEE variability in the model primarily through the impact of growing season length on length of carbon uptake period. These results also suggest that timescales over which climate impacts decomposition and respiration is longer, which is not surprising given the longer residence time of carbon in decomposing pools (soil) versus photosynthetic pools (leaves). The model also highlighted the role that climate

variability imparts on carbon flux spatial coherence, at least on length scales of 100 km, though this question would be best further explored with a larger scale geostatistical study of carbon flux spatial variation.

Old-growth forest and wetland annual carbon flux variability were less well simulated, suggesting a strong role for internal biotic dynamics and moisture variability on carbon flux variations at some sites. These dynamics may be an important aspect of regional carbon cycle variability, especially as forests in the region age and long-term drought conditions persist. Other noted causes of IAV that also require further consideration, especially at regional scales, include the role of stochastic disturbance (Desai *et al.*, 2007), pest outbreaks (Cook *et al.*, 2008), and internal organic matter decomposition dynamics (Ricciuto *et al.*, 2008).

The impact of climate variability on phenology and ultimately ecosystem biogeochemistry is a first order climate-ecosystem interaction, and of likely importance on the predictability of future carbon cycles as anthropogenic climatic changes are expected to be strongly felt in mid-continental mid-latitude regions. Preliminary findings from long term flux tower observations and careful ecosystem model parameterization in a boreal-temperate transition region suggest that future climate change in the shoulder seasons is likely to affect the carbon balance of mixed and deciduous broadleaf forests, perhaps more than climatic changes occurring in the central part of the growing season. However, these findings are limited by lack of longer-term carbon cycle and phenological observations. Additionally, the variety of findings among montaine, grassland, temperate, boreal, and temperate-boreal transition regions highlight the need for continued efforts to better parameterize climate sensitivity of phenology in ecosystem models.

Acknowledgements

Flux tower observations could not have been made without the assistance of those associated with the Chequamagon Ecosystem-Atmosphere Study (ChEAS), especially K. Davis of The Pennsylvania State University, J. Thom and S. Knuth of University of Wisconsin-Madison, B. Cook of NASA Goddard Space Flight Center, D. Ricciuto of Oak Ridge National Labs, P. Curtis of The Ohio State University, C. Gough of Virginia Commonwealth University, C. Vogel of University of Michigan Biological Station, R. Teclaw and D. Baumann of the U.S. Forest Service Northern Research Station, and R. Strand, of the Wisconsin Education Communications Board (ECB). I also would like to thank B. Sacks, University of Wisconsin-Madison for discussion of parameter estimation techniques and the Center for Climatic Research (CCR) for support. This work was supported by the Department of Energy (DOE) Office of Biological and Environmental Research (BER) National Institute for Climatic Change Research (NICCR) Midwestern Region Subagreement 050516Z19 and the National Science Foundation (NSF) Biology Directorate Grant DEB-0845166.

References

Baldocchi, D. D., *et al.* (2001), FLUXNET: A new tool to study the temporal and spatial variability of ecosystem-scale carbon dioxide, water vapor, and energy flux densities. *Bull. Amer. Meteorol. Soc.*, *82*, 2415-2434.

Baldochhi, D. D., *et al.* (2005), Predicting the onset of net carbon uptake by deciduous forests with soil temperature and climate data: a synthesis of FLUXNET data. *International J. Biometeorol.*, *49*, 377-387.

Barr A.G., *et al.* (2006), Climatic controls on the carbon and water balances of a boreal aspen forest, 1994-2003, *Global Change Biol.*, *13*, 561–576.

Bonan, G. B. (2008), Forests and climate change: Forcings, feedbacks, and the climate benefits of forests, *Science*, *320*(5882), 1444-1449, doi:10.1126/science.1155121.

Braswell, B. H., B. Sacks, E. Linder, and D. S. Schimel (2005), Estimating ecosystem process parameters by assimilation of eddy flux observations of NEE. *Global Change Biol.*, 11, 335-355.

Carvalhais, N., *et al.* (2008), Implications of the carbon cycle steady state assumption for biogeochemical modeling performance and inverse parameter retrieval, *Global Biogeochem. Cy*., *22*, GB2007, doi:10.1029/2007GB003033.

Chen W. J., *et al.* (1999), Effects of climatic variability on the annual carbon sequestration by a boreal aspen forest, *Global Change Biol.*, *5*, 41–53.

Churkina, G., D. Schimel, B. H. Braswell, and X. M. Xiao (2005), Spatial analysis of growing season length control on net ecosystem exchange. *Global Change Biol.*, *11*, 1777-1787.

Cook, B. D., *et al.* (2004), Carbon exchange and venting anomalies in an upland deciduous forest in northern Wisconsin, USA, *Agric. For. Meteorol.*, *126*, 271-295.

Cook, B. D., P. V. Bolstad, J. G. Martin, F. A. Heinsch, K. J. Davis, W. Wang, A. R. Desai, and R. M. Teclaw (2008), Using light-use and production efficiency models to predict forest production and carbon exchange during canopy disturbance events, *Ecosystems*, *11*, 26-44, doi:10.1007/s10021-007-9105-0.

Davis, K. J., *et al.*, (2003), The annual cycle of CO_2 and H_2O exchange over a northern mixed forest as observed from a very tall tower, *Global Change Biol.*, 9, 1278-1293.

518 Desai, A. R., P. V. Bolstad, B. D. Cook, K. J. Davis, and E. V. Carey (2005), Comparing net
519 ecosystem exchange of carbon dioxide between an old-growth and mature forest in the
520 upper Midwest, USA, *Agric. For. Meteorol, 128*(1-2), 33-55,
521 doi:10.1016/j.agformet.2004.09.005.
522 Desai, A. R., P. R. Moorcroft, P. V. Bolstad, and K. J. Davis (2007), Regional carbon fluxes
523 from a biometrically-constrained dynamic ecosystem model: Impact of disturbance, CO_2
524 fertilization and heterogeneous land cover, *J. Geophys. Res*, *112*(G01017),
525 doi:10.1029/2006JG000264.
526 Desai, A. R., *et al.* (2008), Influence of vegetation and seasonal forcing on carbon dioxide fluxes
527 across the Upper Midwest, USA: Implications for regional scaling, *Agric. For. Meteorol.*,
528 *148*(2), 288-308, doi:10.1016/j.agrformet.2007.08.001.
529 Desai, A. R., B. R. Helliker, P. R. Moorcroft, A. E. Andrews, and J. A. Berry (2010), Climatic
530 controls of interannual variability in regional carbon fluxes from top-down and bottom-
531 up perspectives, *J. Geophys. Res.*, 115, G02011, doi:10.1029/2009JG001122.
532 Dunn A.L., C. C. Barford, S. C. Wofsy, M. L. Goulden, B. C. Daube, (2007) A long-term record
533 of carbon exchange in a boreal blackspruce forest: means, responses to interannual
534 variability, and decadal trends, *Global Change Biol.*, *13*, 577–590.
535 Gordo, O. and J. J. Sanz (2010), Impact of climate change on plant phenology in Mediterranean
536 ecosystems, *Global Change Biol.*, *16*, 1082-1106, doi:10.1111/j.1365-
537 2486.2009.02084.x.
538 Gough C. M., C. S. Vogel, H.-P. Schmid, H.-B. Su, and P. S. Curtis (2008), Multi-year
539 convergence of biometric and meteorological estimates of forest carbon storage, *Agric.*
540 *For. Meteorol*, *148*, 158-170.

541 Goulden M.L., J. W. Munger, S.M. Fan, B. C. Daube, S. C. Wofsy (1996), Exchange of carbon
542 dioxide by a deciduous forest: response to interannual climate variability, *Science*, *271*,
543 1576–1578.
544 Hollinger D. Y., J. Aber, B. Dail, S. M. Davidson, H. Goltz, and H. Hughes (2004), Spatial and
545 temporal variability in forest-atmosphere CO2 exchange, *Global Change Biol.*, *10*, 1689–
546 1706.
547 Hu, J., D. J. P. Moore, S. P. Burns, and R. K. Monson (2010), Longer growing seasons lead to
548 less carbon sequestration by a subalpine forest, *Global Change Biol.*, *16*, 771-783,
549 doi:10.1111/j.1365-2486.2009.01967.x.
550 Linderholmm H. W. (2006), Growing season changes in the last century. *Agric. For. Meteorol.*,
551 *137*, 1-14.
552 Luo, Y. Q., E. S. Weng, X. W. Wu, C. Gao, X. H. Zhou, and L. Zhang (2009), Parameter
553 identifiability, constraint, and equifinality in data assimilation with ecosystem models,
554 *Ecol. Apps.*, *19*, 571-57.
555 Menzel, A. and P. Fabian (1999), Growing season extended in Europe. *Nature*, *455*, 213-215.
556 Metropolis, N., and S. Ulam (1949), The Monte Carlo method, *J. Am. Stat. Assoc.*, *44*, 335-341.
557 Moffat, A. M., *et al.* (2007), Comprehensive comparison of gap filling techniques for eddy
558 covariance net carbon fluxes, *Agric. For. Meteorol., 147***,** 209-232.
559 Morisette, J.T., *et al.* (2009), Tracking the rhythm of the seasons in the face of global change:
560 phenological research in the 21st Century. *Frontiers in Ecology and the Environment*, 7:
561 253-260, doi: 10.1890/070217.
562 Myneni, R. B., C. D. Keeling, C. J. Tucker, G. Asrar, and R. R. Nemani (1997), Increasing plant
563 growth in the northern high latitudes from 1981 to 1991. *Nature, 386*, 698-702.

564 Peñuelas, J., T. Rutishauser, and I. Filella (2009), Phenology feedbacks on climate change,
565 *Science*, *324*(5929), 887-888, doi:10.1126/science.1173004.
566 Piao, S. *et al.* (2008), Net carbon dioxide losses of northern ecosystems in response to autumn
567 warming, *Nature*, *451*, 49-53.
568 Polley, H. W., *et al.* (2010), Physiological and environmental regulation of interannual
569 variability in CO2 exchange on rangelands in the western United States, *Global Change*
570 *Biol.*, *16*, 990-1002, doi:10.1111/j.1365-2486.2009.01966.x.
571 Ricciuto, D. M., M. P. Butler, K. J. Davis, B. D. Cook, P. S. Bakwin, A. Andrews, and R. M.
572 Teclaw (2008), Causes of interannual variability in ecosystem–atmosphere CO_2 exchange
573 in a northern Wisconsin forest using a Bayesian model calibration, *Agric. For. Meteorol.*,
574 *148*(2), 309-327.
575 Richardson, A. D., A. S. Bailey, E. G. Denny, C. W. Martin, and J. O'Keefe (2006), Phenology
576 of a northern hardwood forest canopy, *Global Change Biol.*, *12*, 1174-1178.
577 Richardson A.D., D. Y. Hollinger, J. D. Aber, S. V. Ollinger, B. H. Braswell (2007),
578 Environmental variation is directly responsible for short- but not long-term variation in
579 forest-atmosphere carbon exchange, *Global Change Biol.*, *13*, 788–803.
580 Richardson, A. D., D. Y. Hollinger, D. B. Dail, J. T. Lee, J. W. Munger, and J. O'Keefe (2009),
581 Influence of spring phenology on seasonal and annual carbon balance in two contrasting
582 New England forests, *Tree Phys.*, *29*, 321-331, doi:10.1093/treephys/tpn040.
583 Sacks, W. J., D. S. Schimel, R. K. Monson, and B. H. Braswell (2006), Model-data synthesis of
584 diurnal and seasonal CO_2 fluxes at Niwot Ridge, Colorado, *Global Change Biol.*, *12*(2),
585 240-259.

586 Sierra, C., H. W. Loescher, M. E. Harmon, A. D. Richardson, D. Y. Hollinger, and S. S. Perakis
587 (2009), Interannual variation of carbon fluxes from three contrasting evergreen forests:
588 the role of forest dynamics and climate, *Ecology*, *90*(10), 2711-2723.
589 Stine, A.R., P. Huybers, and I. Y. Fung (2009), Changes in the phase of the annual cycle of
590 surface temperature, *Nature*, *457,* 435-441, doi:10.1038/nature07675.
591 Stöckli, R. and P. L. Vidale (2004), European plant phenology and climate as seen in a 20-year
592 AVHRR land-surface parameter dataset. *International J. Rem. Sens.*, *25*, 3303-3330.
593 Stoy, P. C., *et al.* (2009), Biosphere-atmosphere exchange of CO_2 in relation to climate: a cross-
594 biome analysis across multiple time scales, *Biogeosciences*, *6*, 2297-2312.
595 Sulman, B. N., A. R. Desai, B. D. Cook, N. Saliendra, and D. S. Mackay (2009), Contrasting
596 carbon dioxide fluxes between a drying shrub wetland in Northern Wisconsin, USA, and
597 nearby forests, *Biogeosciences*, *6*, 1115-1126.
598 Urbanski, S., *et al.* (2007), Factors controlling CO2 exchange on timescales from hourly to
599 decadal at Harvard Forest, *J. Geophys. Res.*, *112(G2)*, G02020, doi:
600 10.1029/2006JG000293.
601 Vitasse, Y., A. J. Porte, A. Kremer, R. Michalet, and S. Delzon (2009), Responses of canopy
602 duration to temperature changes in four temperate tree species: relative contributions of
603 spring and autumn leaf phenology. *Oecologia*, *161*, 187-198.
604 Yuan, W., *et al.* (2009), Latitudinal patterns of magnitude and interannual variability in net
605 ecosystem exchange regulated by biological and environmental variables, *Global Change*
606 *Biol.*, *15*, 2905-2920, doi:10.1111/j.1365-2486.2009.01870.x.
607

608 White, M. A., *et al.* (2009) Intercomparison, interpretation, and assessment of spring phenology
609 in North America estimated from remote sensing for 1982-2006. *Global Change Biol*.,
610 *15*, 2335-2359.
611

Figure captions

Figure 1. Map of north-central United States showing location of the five flux tower sites used in this study.

Figure 2. Ensemble average cumulative daily NEE for observations, and the three model experiments (A_H, A_I, and S). Averages were performed over the observed record noted in Table 1. The model generally captured the seasonal pattern of NEE at all sites, with worst performance at US-Syv and US-PFa. Observed and model uncertainty is not shown to preserve clarity, but generally fall within 10% of any observation.

Figure 3. Observed standardized interannual variability in NEE at the five study sites. Strong coherence in variability in NEE was observed across the time period, even though absolute magnitudes in NEE variability varied widely. Observational uncertainty in NEE is noted by the horizontal bars.

Figure 4. Correlation of anomalies in observed and modeled annual NEE using a) the A_H cost function parameters (Table 4) and b) the A_I cost function parameters (Table 5). Significant improvement in simulation of interannual variability was found for all sites in the latter.

Figure 5. Comparison of observed light extinction profile derived leaf on (square) and leaf off (triangle) date anomalies to IFUSE model for the US-WCr site, using the A_I parameters. Generally, variability in both dates was modestly well simulated, though the slope of leaf off appears too steep, while the leaf on dates mostly fall on the 1:1 line except for one outlier.

634

635 **Figure 6.** Same as Fig. 4 but for the S cost function parameters (Table 6). Interannual variations
636 by the S model were well simulated for most sites, but less successfully for US-UMB and quite
637 poorly for US-Syv.

638

639 **Figure 7.** Linear regression derived slope of the relationship between annual NEE and anomaly
640 in dates of leaf on (L_{ON}), leaf off (L_{OFF}) and growing season length (G_{SL}) as quantified from
641 IFUSE model output using A_I cost function parameters (Table 5) plotted against linear
642 correlation of this relationship at all sites. Dotted line indicates $p<0.1$ significance level.

Tables

Table 1. Location and types of co-located eddy covariance flux towers and time periods analyzed in this study along with their mean annual NEE and uncertainty in gC m^{-2} yr^{-1}, 1-σ IAV in gC m^{-2} yr^{-1}, post-filtering total gap fraction, and reference. Data gaps were strongly skewed toward nighttime data due to low turbulence screening criteria.

Name	Location	Type	Years	NEE	IAV	% Gaps	Reference
US-WCr	45° 48' N 90° 5' W	Forest	2000-2006	-380 ± 29	149	51%	Cook *et al.*, 2004
US-UMB	45° 34' N 84° 43' W	Forest	1999-2003	-284 +/- 22	43	39%	Gough *et al.*, 2008
US-Syv	46° 14'N 89° 21' W	Forest	2002-2006	1 ± 18	112	48%	Desai *et al.*, 2005
US-Los	46° 5' N 89° 59' W	Wetland	2001-2006	-84 ± 10	16	32%	Sulman *et al.*, 2009
US-PFa	45° 57' N 90° 16' W	Mixed	1997-2005	111 ± 21	67	28%	Ricciuto *et al.*, 2008

Table 2. Model parameters definitions, prior values, and acceptable posterior parameter ranges used by the IFUSE model and MCMC parameterization.

Name	Definition	Value
Fixed parameters		
k	Light extinction coefficient	0.5 FIXED
LAI_{min}	Minimum leaf area	US-WCr 0.0, US-UMB 0.0, US-Syl 0.5, US-Los 0.0, US-PFa 0.5
LAI_{max}	Maximum leaf area	US-WCr 5.3, US-UMB 3.7, US-Syl 4.1, US-Los 4.9, US-PFa 3.7
Phenology parameters		
α	Leaf on (L_{ON}) slope	0.05 (0.05-0.5)
GDD_{thresh}	Growing degree day threshold	200 (10-400)
β	Leaf off (L_{OFF}) slope	0.1 (0.05-0.5)
$TEMP_{thresh}$	Soil temperature threshold	4 (0-20)
Photosynthesis parameters		
LUE	Light use efficiency	0.25 (0-1)
T_{min}	Minimum photosynthetic temperature	0 (-15-10)
T_{opt}	Optimum photosynthetic temperature	15 (5-40)
VPD_{max}	Maximum photosynthetic VPD	3000 (0-20000)
VPD_{min}	Minimum photosynthetic VPD	100 (0-2000)
Respiration parameters		
r_s	Basal maintenance respiration	2 (0.1-5)
r_v	Basal growth respiration	2 (0.1-5)
b_1	Maintenance respiration rate	0.03 (0-0.5)
b_2	Growth respiration rate	0.03 (0-0.25)
b_3	Leaf respiration fraction	0.05 (0-0.25)

651 **Table 3.** Percent of variance explained (r^2) and mean absolute error (MAE) of observed NEE anomalies against the model in
652 asynchronous half-daily cost function (A_H), asynchronous interannual cost function (A_I), and synchronous (S) experiments. All
653 experiments were able to significantly capture daily variations NEE ($p<0.01$), but A_I captured interannual variability at the most
654 number of sites, followed by the S. All correlations at the half-daily scale were significant, while significance of model-data
655 correlations of interannual variability are marked by *** ($p<0.01$), ** ($p<0.05$), and * ($p<0.1$).

		Model	US-WCr	US-UMB	US-Syv	US-Los	US-PFa
Half-daily	r^2	A_H	0.90	0.93	0.87	0.88	0.83
		A_I	0.81	0.82	0.84	0.85	0.77
		S	0.81	0.88	0.73	0.82	0.77
	MAE	A_H	0.48	0.43	0.50	0.31	0.46
		A_I	0.78	0.59	0.53	0.37	0.55
		S	0.83	0.52	0.64	0.40	0.53
Inter-Annual	r^2	A_H	0.17	0.44	0.00	0.53	0.38
		A_I	0.87***	0.87**	0.69	0.76*	0.78**
		S	0.89***	0.64	0.24	0.88**	0.77**
	MAE	A_H	109	28	95	12	39
		A_I	58	11	48	6	26
		S	46	31	71	9	25

656

657

Table 4. Best and range of accepted posterior model parameters for each site using the asynchronous half-daily cost function (A_H).

Name	US-WCr	US-UMB	US-Syv	US-Los	US-PFa
Phenology parameters					
α	0.089 (0.085-0.094)	0.142 (0.122-0.156)	0.195 (0.154-0.283)	0.206 (0.186-0.219)	0.160 (0.130-0.185)
GDD_{thresh}	154.0 (153.8-156.1)	107.1 (102.1-111.3)	81.1 (77.3-84.9)	80.7 (79.9-80.8)	131.5 (131.2-131.6)
β	0.182 (0.155-0.200)	0.165 (0.138-0.198)	0.098 (0.074-0.147)	0.091 (0.070-0.108)	0.135 (0.082-0.199)
$TEMP_{thresh}$	11.3 (11.1-11.8)	9.0 (8.9-9.2)	9.6 (9.2-11.1)	11.4 (11.3-11.4)	10.2 (9.2-10.9)
Photosynthesis parameters					
LUE	0.273 (0.262-0.281)	0.441 (0.326-0.444)	0.286 (0.265-0.371)	0.195 (0.187-0.251)	0.193 (0.179-0.200)
T_{min}	-5.6 (-15.0-1.7)	-15.0 (-15.0--14.2)	-14.0 (-15.0--10.7)	-11.0 (-14.9--7.1)	-3.5 (-7.7-0.4)
T_{opt}	6.7 (5.0-9.2)	39.1 (27.1-40.0)	29.5 (27.2-40.0)	32.1 (29.7-40.0)	11.0 (7.9-12.8)
VPD_{max}	4125 (3797-4562)	3143 (3016-3292)	3565 (3291-3908)	3893 (3636-4344)	3571 (3223-3929)
VPD_{min}	2 (0-115)	73 (0-309)	18 (0-235)	421 (15-513)	0 (0-201)
Respiration parameters					
r_s	1.01 (0.76-1.17)	0.11 (0.10-0.25)	0.12 (0.10-0.37)	0.55 (0.40-0.70)	0.73 (0.51-0.99)
r_v	0.22 (0.11-0.45)	0.95 (0.83-1.00)	1.55 (1.32-1.68)	0.65 (0.53-0.74)	0.71 (0.54-0.90)
b_1	0.0954 (0.0763-0.1238)	0.3812 (0.2634-0.4216)	0.1595 (0.0204-0.3538)	0.1091 (0.0923-0.1343)	0.1111 (0.0840-0.1405)
b_2	0.0275 (0.0002-0.0806)	0.0438 (0.0349-0.0499)	0.0811 (0.0730-0.0927)	0.0879 (0.0757-0.0983)	0.0872 (0.0723-0.1066)
b_3	0.0001 (0.0000-0.0052)	0.0007 (0.0000-0.0112)	0.0001 (0.0000-0.0391)	0.0121 (0.0001-0.0299)	0.0995 (0.0655-0.1221)

Table 5. Same as Table 4 but for the asynchronous interannual cost function (A_I).

Name	US-WCr	US-UMB	US-Syv	US-Los	US-PFa
Phenology parameters					
α	0.093 (0.084-0.097)	0.500 (0.467-0.500)	0.130 (0.113-0.139)	0.249 (0.245-0.251)	0.050 (0.050-0.051)
GDD_{thresh}	130.2 (127.6-130.3)	71.5 (71.4-71.5)	56.4 (56.3-56.9)	58.2 (57.1-58.4)	149.6 (149.4-149.8)
β	0.490 (0.317-0.500)	0.050 (0.050-0.053)	0.051 (0.050-0.059)	0.476 (0.450-0.483)	0.050 (0.050-0.050)
$TEMP_{thresh}$	1.4 (1.4-1.4)	-7.4 (-8.0--6.8)	14.6 (14.5-14.7)	8.3 (8.1-8.5)	-5.6 (-6.9--5.1)
Photosynthesis parameters					
LUE	0.463 (0.444-0.483)	0.204 (0.202-0.205)	0.244 (0.231-0.250)	0.183 (0.179-0.188)	0.159 (0.156-0.162)
T_{min}	-0.2 (-0.3--0.2)	8.9 (8.8-9.0)	6.7 (6.7-6.8)	-4.1 (-4.1--4.0)	5.0 (5.0-5.0)
T_{opt}	36.3 (34.6-37.8)	19.6 (19.5-19.7)	7.0 (6.9-7.0)	30.7 (30.3-31.5)	5.1 (5.1-5.2)
VPD_{max}	19802 (15935-19998)	2230 (2184-2301)	3681 (3489-3930)	4074 (3874-4314)	13304 (2110-19973)
VPD_{min}	10 (0-239)	1536 (1506-1549)	3 (0-209)	542 (480-603)	1964 (1732-1999)
Respiration parameters					
r_s	0.23 (0.22-0.24)	0.81 (0.78-0.81)	1.29 (1.21-1.41)	0.31 (0.28-0.33)	0.59 (0.55-0.63)
r_v	1.06 (1.04-1.12)	0.10 (0.10-0.12)	0.97 (0.86-1.05)	0.89 (0.86-0.92)	1.43 (1.39-1.47)
b_1	0.4999 (0.4979-0.5000)	0.0449 (0.0414-0.0449)	0.1395 (0.1330-0.1461)	0.1859 (0.1729-0.2043)	0.0897 (0.0824-0.0944)
b_2	0.0001 (0.0000-0.0011)	0.0002 (0.0000-0.0184)	0.0001 (0.0000-0.0020)	0.0769 (0.0745-0.0797)	0.0836 (0.0798-0.0883)
b_3	0.0000 (0.0000-0.0010)	0.0005 (0.0000-0.0044)	0.0002 (0.0000-0.0066)	0.0004 (0.0000-0.0058)	0.0000 (0.0000-0.0016)

661 **Table 6.** Same as Table 4, but for the synchronous cost function (S).

Name	US-WCr	US-UMB	US-Syv	US-Los	US-PFa
Phenology parameters (jointly-optimized)					
α	0.063 (0.061-0.065)				
GDD_{thresh}	165.3 (165.2-165.3)				
β	0.100 (0.084-0.112)				
$TEMP_{thresh}$	4.8 (4.7-4.8)				
Photosynthesis parameters					
LUE	0.299 (0.295-0.305)	0.495 (0.479-0.520)	0.300 (0.289-0.310)	0.260 (0.251-0.276)	0.159 (0.154-0.162)
T_{min}	4.0 (4.0-4.0)	-2.8 (-3.0--2.0)	9.4 (9.4-9.5)	2.7 (2.7-3.0)	-4.0 (-4.7--3.9)
T_{opt}	21.3 (21.0-21.6)	38.1 (36.9-39.9)	21.2 (21.0-21.8)	37.8 (36.4-40.0)	20.5 (19.4-21.2)
VPD_{max}	11931 (2010-19999)	3399 (3279-3647)	3389 (3261-3530)	4028 (3339-4565)	11206 (2442-19991)
VPD_{min}	1981 (1647-1999)	287 (99-369)	144 (10-229)	760 (721-956)	1943 (1084-1999)
Respiration parameters					
r_s	0.23 (0.22-0.24)	0.90 (0.81-0.92)	1.79 (1.74-1.81)	0.31 (0.28-0.52)	0.35 (0.26-0.45)
r_v	1.26 (1.23-1.29)	0.34 (0.30-0.39)	0.10 (0.10-0.12)	0.91 (0.71-0.93)	1.31 (1.26-1.37)
b_1	0.4999 (0.4984-0.5000)	0.1073 (0.0987-0.1165)	0.2103 (0.2032-0.2146)	0.2720 (0.1780-0.3230)	0.2689 (0.2058-0.3217)
b_2	0.0000 (0.0000-0.0009)	0.0002 (0.0000-0.0058)	0.0014 (0.0000-0.0187)	0.0859 (0.0635-0.0885)	0.0932 (0.0867-0.0991)
b_3	0.0000 (0.0000-0.0005)	0.0003 (0.0000-0.0050)	0.0000 (0.0000-0.0035)	0.0004 (0.0000-0.0245)	0.0014 (0.0000-0.0142)

662

Figures

Figure 1. Map of north-central United States showing location of the five flux tower sites used in this study.

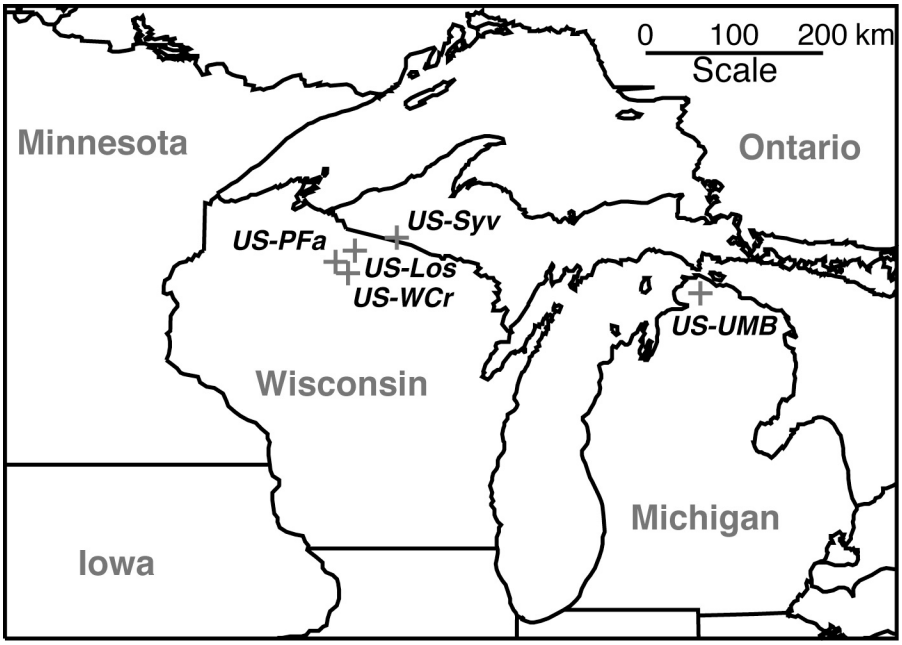

667 **Figure 2.** Ensemble average cumulative daily NEE for observations, and the three model
668 experiments (A_H, A_I, and S). Averages were performed over the observed record noted in Table
669 1. The model generally captured the seasonal pattern of NEE at all sites, with worst performance
670 at US-Syv and US-PFa. Observed and model uncertainty is not shown to preserve clarity, but
671 generally fall within 10% of any observation.

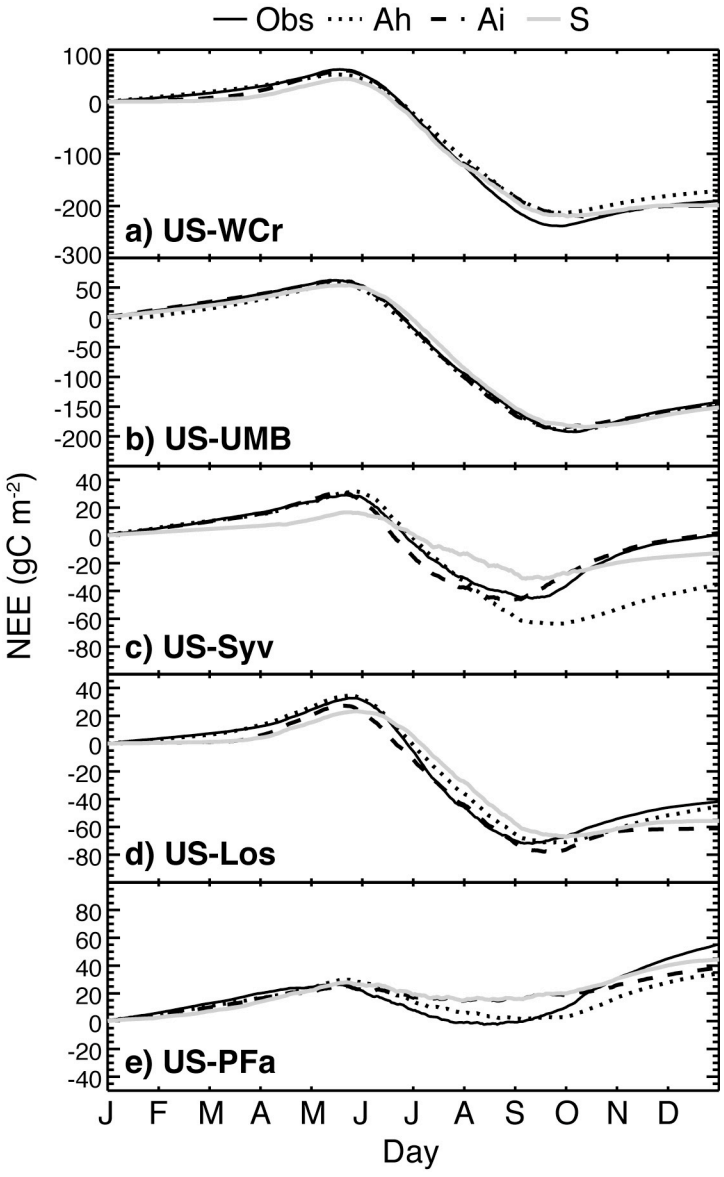

672

673 **Figure 3.** Observed standardized interannual variability in NEE at the five study sites. Strong
674 coherence in variability in NEE was observed across the time period, even though absolute
675 magnitudes in NEE variability varied widely. Observational uncertainty in NEE is noted by the
676 horizontal bars.

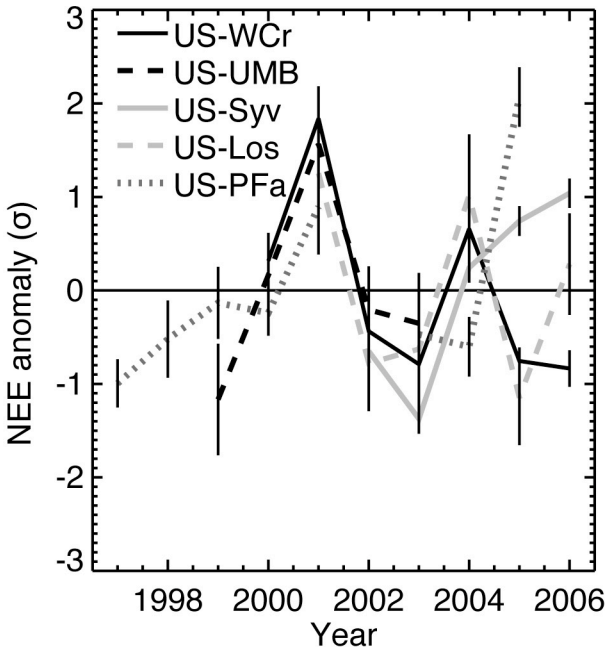

677

678

678 **Figure 4.** Correlation of anomalies in observed and modeled annual NEE using a) the A_H cost
679 function parameters (Table 4) and b) the A_I cost function parameters (Table 5). Significant
680 improvement in simulation of interannual variability was found for all sites in the latter.

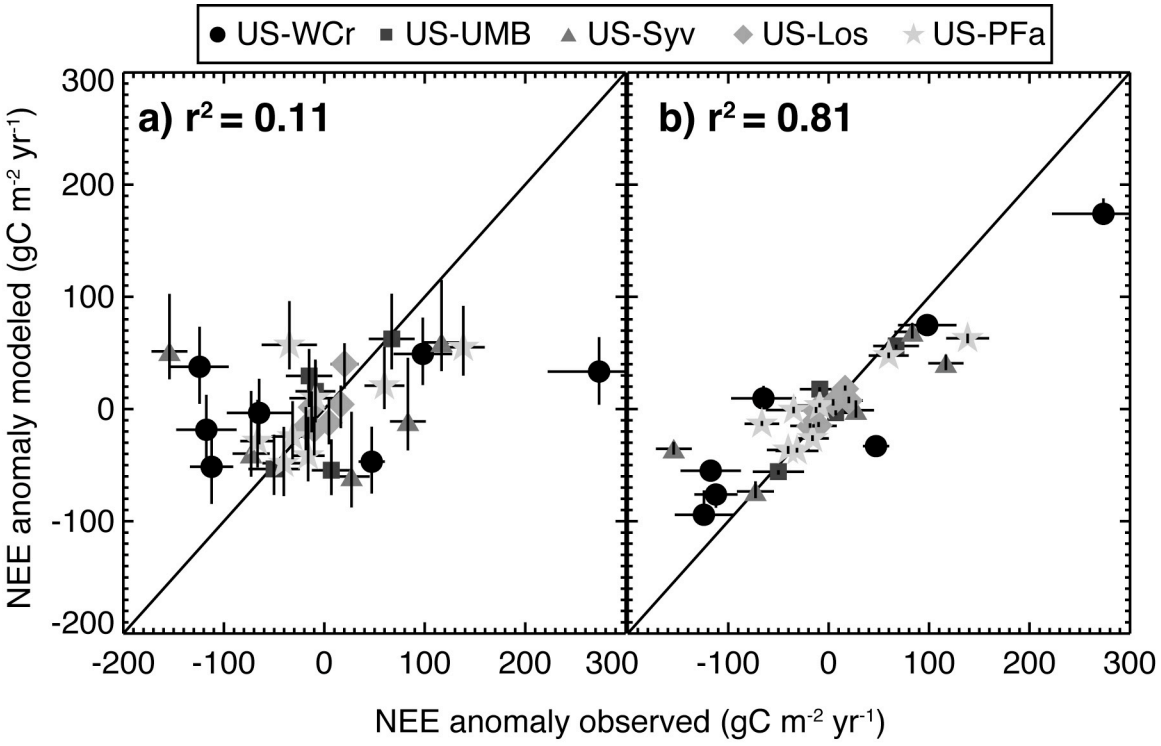

681

682

682 **Figure 5.** Comparison of observed light extinction profile derived leaf on (square) and leaf off
683 (triangle) date anomalies to IFUSE model for the US-WCr site, using the A_I parameters.
684 Generally, variability in both dates was modestly well simulated, though the slope of leaf off
685 appears too steep, while the leaf on dates mostly fall on the 1:1 line except for one outlier.

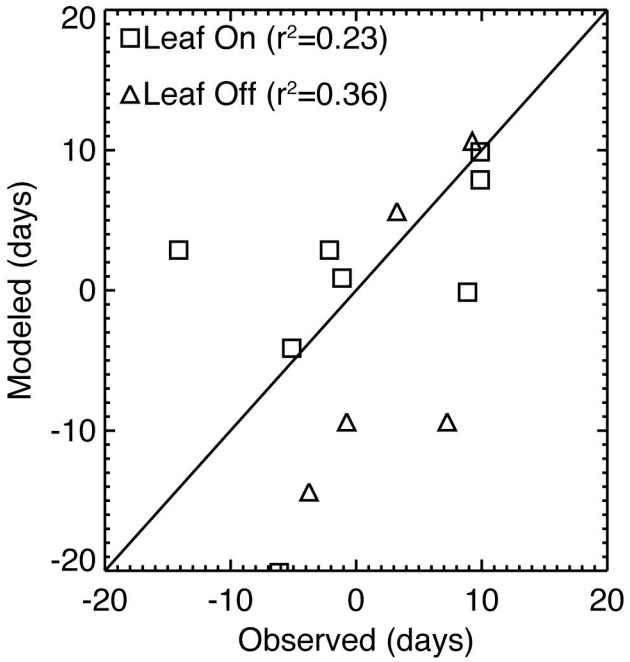

686

687

687 **Figure 6.** Same as Fig. 4 but for the S cost function parameters (Table 6). Interannual variations
688 by the S model were well simulated for most sites, but less successfully for US-UMB and quite
689 poorly for US-Syv.

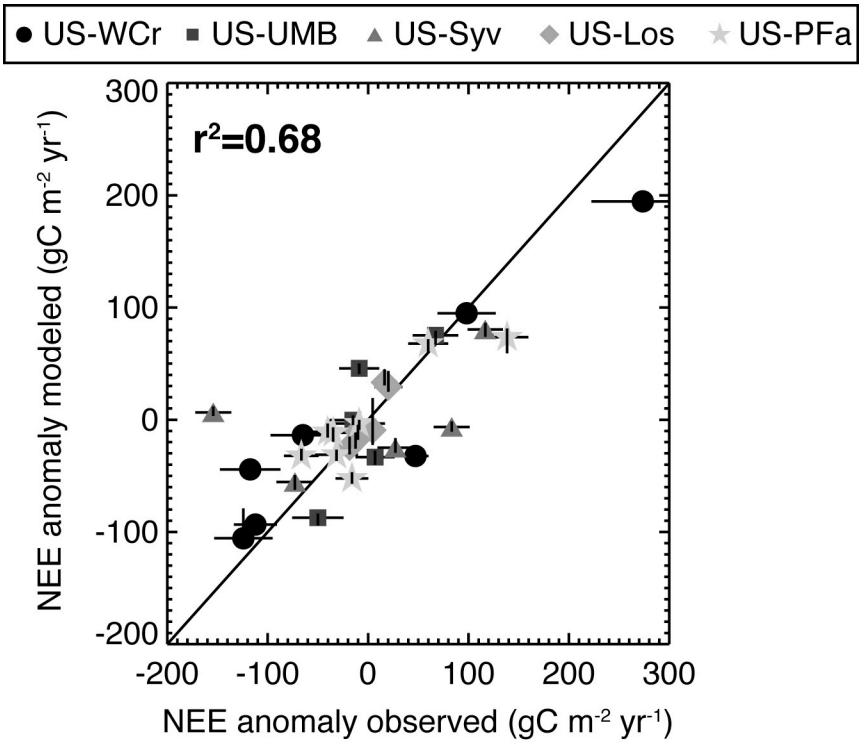

690

691

691 **Figure 7.** Linear regression derived slope of the relationship between annual NEE and anomaly
692 in dates of leaf on (L_{ON}), leaf off (L_{OFF}) and growing season length (G_{SL}) as quantified from
693 IFUSE model output using A_I cost function parameters (Table 5) plotted against linear
694 correlation of this relationship at all sites. Dotted line indicates $p<0.1$ significance level.

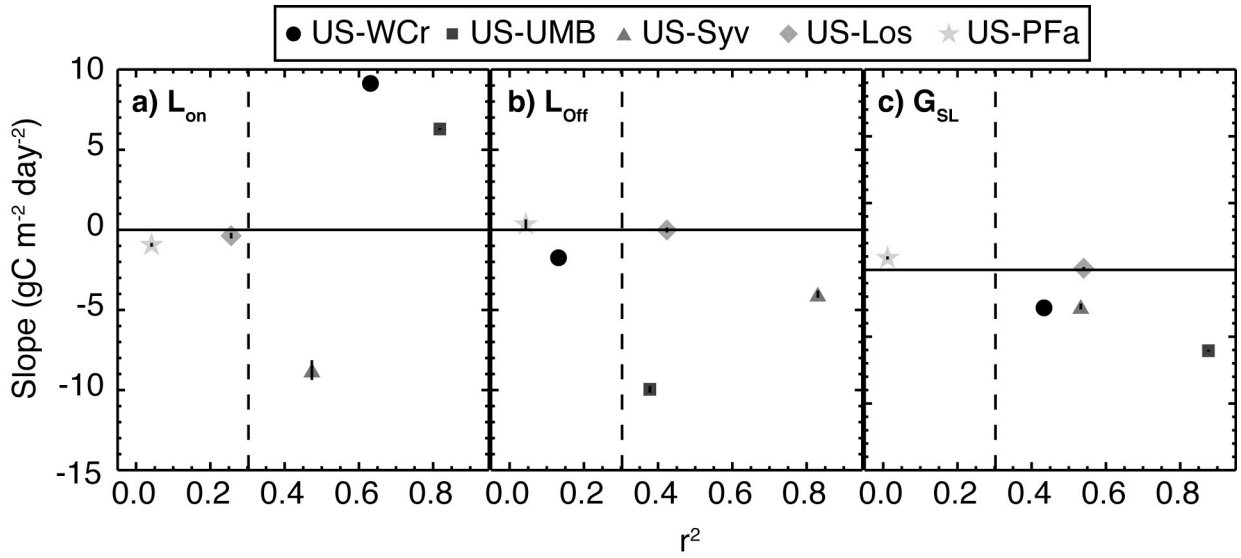

695